Ultrasonics Sonochemistry 88 (2022) 106100

Contents lists available at ScienceDirect

Ultrasonics Sonochemistry

journal homepage: www.elsevier.com/locate/ultson

Ultrasound enhanced butyric acid-lauric acid designer lipid synthesis: Based on artificial neural network and changes in enzymatic structure

Wangxin Liu [a], Xianliang Luo [a], Yang Tao [d], Ying Huang [a], Minjie Zhao [a], Jiahui Yu [c], Fengqin Feng [a,b,*], Wei Wei [c,*]

[a] College of Biosystems Engineering and Food Science, Zhejiang University, Hangzhou 310058, China
[b] ZhongYuan Institute, Zhejiang University, Hangzhou 310058, China
[c] State Key Lab of Food Science and Technology and Collaborative Innovation Center of Food Safety and Quality Control, Jiangnan University, Wuxi 214122, China
[d] College of Food Science and Technology, Nanjing Agricultural University, Nanjing 210095, China

ARTICLE INFO

Keywords:
Butyrate acid
Laurate acid
Designer lipid
Ultrasound
Artificial neural network
Enzymatic structure

ABSTRACT

Ultrasound is a green technology for intensifying enzymatic reactions. In this study, an ultrasonic water bath with equipment parameters of 28 kHz, 1750.1 W/m^2, 60% duty cycle was used to assist the synthesis of butyric acid-lauric acid designer lipid (BLDL), which was catalyzed by Lipozyme 435. A convincing three-layer feed-forward artificial neural network (ANN) model was established (R^2 = 0.949, RMSE = 4.759, ADD = 7.329) to accurately predict the optimal parameters combination, which was described as 13.72 mL reaction volume, 15.49% enzyme loading, 0.253 substrate molar ratio (tributyrin/lauric acid), 56.58 °C reaction temperature and 120 min reaction time. The ultrasonic assistance increased actual butyric acid conversion rate by 11.38%, and also enhanced the consumption rate of tributyrin and lauric acid during the reaction. Meanwhile, the esterification activity of Lipozyme 435 was enhanced and its effectiveness up to 6 cycles. Structurally, ultrasound assistance significantly disrupted the secondary structure of the Lipozyme 435: reduced the content of α-helices, increased the content of β-sheet and β-turn. In addition, sonication caused an increase in crevice and micro-damage on the surface of the immobilized enzyme. In conclusion, low-intensity ultrasound at 28 kHz improved the synthesis efficiency of BLDL, which was scientifically predicted by ANN model, and the change of enzyme structure may be the vital reason for ultrasound enhanced reaction. However, the effect of ultrasound on immobilized enzymes' activity needs to be further explored.

1. Introduction

Designer lipids are novel lipids formed by artificially altering the fatty acid (FA) composition or its position on the glycerol backbone, which often have superior organoleptic properties and are more health-friendly than natural lipids. Nowadays, designer lipids are widely applied in food, nutraceutical and pharmaceutical industries, such as baby food, diet food and anti-cardiovascular products [1]. Wei et al. synthesized 1,3-dioleoyl-2-palmitoylglycerol (OPO) through the catalysis of Lipozyme RM IM using tripalmitin and oleic acid as raw materials, the designer lipid can improve the symptoms of energy deficiency, calcium deficiency and constipation in infants [2]. Another study documented that designer lipid synthesized from palm olein and caprylic acid has lower viscosity, lighter color and better thermo-oxidative stability [3]. Due to the multiple health benefits and processing properties of designer lipids, there is an increasing need for greener and more effective designer lipids synthesis methods.

Traditionally, acid hydrolysis is an ideal method to change the FA composition on the glycerol backbone to form new designer lipids [4]. Nevertheless, the acid hydrolysis transesterification catalyzed by

Abbreviations: FA, fatty acid; OPO, 1,3-dioleoyl-2-palmitoylglycerol; MCFA, medium chain fatty acid; BLDL, butyric acid-lauric acid designer lipid; ANN, artificial neural network; GA, genetic algorithm; CCD, central composite design; R^2, coefficient of determination; RMSE, root mean square error; AAD, absolute mean deviation; FT-IR, Fourier transform infrared spectroscopy; CD, circular dichroism; TAG, triacylgycerol; DAG, diacylglycerol; MAG, monoacylglycerol; FFA, free fatty acid.

* Corresponding authors at: College of Biosystems Engineering and Food Science, Zhejiang University, No. 866, Yuhangtang Road, Hangzhou 310058, China (F. Feng). School of Food Science and Technology, Jiangnan University, No. 1800, Lihu Avenue, Wuxi 214122, China (W. Wei).

E-mail addresses: fengfq@zju.edu.cn (F. Feng), weiw@jiangnan.edu.cn (W. Wei).

https://doi.org/10.1016/j.ultsonch.2022.106100
Received 12 June 2022; Received in revised form 10 July 2022; Accepted 19 July 2022
Available online 22 July 2022

chemical catalysts often involves random insertion of fatty acids, and the subsequent purification costs are high, which limit the application of designer lipids. In comparison, immobilized enzymes have the advantages of safety, environmental friendliness, fewer by-products, and easy recycling. For enzymatic reactions, the substrate molar ratio, reaction temperature and enzyme loading are important factors affecting the reaction efficiency. When a variety of substrates with different polarities are mixed in the reaction system, the change of the substrates molar ratio will directly change the polarity of the reaction system, which affect the enzyme activity and mass transfer [5]. In addition, a moderate increase in reaction temperature and enzyme loading may accelerate the reaction, while improper adjustment may bring economic burden and reduce reaction efficiency [6]. Therefore, the optimization of the enzymatic esterification reaction is very important. The artificial neural network (ANN) model is especially suitable for solving complex nonlinear relationship problems, which can reflect the relationship between the independent variable and the dependent variable more accurately than the response surface model [7,8]. At present, ANNs have been widely used to guide the synthesis of biodiesel [7,9]. However, the potential role of ANNs in guiding designer lipid synthesis remains to be explored. For the choice of immobilized lipase, Lipozyme 435 is a commercial enzyme derived from *Candida antarctica* with *sn*-1,3 specificity [10]. Zhang et al. used Lipozyme 435 to catalyze herring oil, caprylic and stearic acids to synthesize designer lipids that can replace butter [10]. Additionally, Lu et al. compared the ability of Lipozyme 435, Novozyme 435, Lipozyme RM IM and Lipozyme TL IM to catalyze the synthesis of medium and long chain triglycerides from soybean oil and medium chain triglycerides [11]. Among them, Lipozyme 435 was the most efficient. However, the immobilized support increases the mass transfer resistance and reduces the catalytic efficiency of the immobilized enzyme. Long reaction time will cause more acyl migration, so it is necessary to shorten the reaction time to reduce the chance of this phenomenon [12]. Therefore, it is meaningful to improve the catalytic efficiency of immobilized enzymes with new technologies.

Ultrasound is a green and economic processing technology, which is widely used in enhancing enzyme-catalyzed reactions with a frequency range of 20 kHz-100 kHz. The propagation of high-amplitude ultrasonic waves in the liquid medium results in micro-bubbles generation and expansion. Subsequently, the shock waves will be generated when the bubbles collapse [13]. Such shock waves create highly turbulent flow in the reaction mixture accompanied by transient high temperatures and pressures, which in turn alter the enzyme structure, disrupt interactions between reaction substrates and facilitate material diffusion [13,14]. Therefore, ultrasonic-assisted enzymatic catalysis is a potential green technology that can improve the yield and reaction efficiency of designer lipids. Ultrasonic enhancement comes from two aspects: one is to enhance mass transfer, and the other is the activation of lipase itself [15]. Liu et al. used ultrasound assisted Lipozyme RM IM (20 kHz, 130 W) to catalyze the synthesis of OPO. They reported that ultrasound enhances the affinity of the enzyme for the substrate, and the apparent kinetic constant of the reaction was 2.52 times higher than that of conventional mechanical stirring [16]. In another study, with the assistance of ultrasound at the condition of 20 kHz, 70% duty cycle and 240 W, the yield of palm olein designer lipid was increased from 28% (conventional process) to 92% within 360 min [3]. Similarly, More et al. obtained higher designer lipid yields than conventional processes with different MCFA and long-chain oils under the combined action of ultrasonic and enzyme [17]. Notably, ultrasonic parameter plays an important role in its assisted enzymatic synthesis. Under the condition of fixed ultrasonic intensity, frequency and duty cycle, the increase of ultrasonic volume will lead to the decrease of energy density, and finally weaken the cavitation effect caused by ultrasonic in the reaction system [18,19]. In addition, ultrasonic duration is also one of the ultrasonic parameters that worthy of attention. Taken together, ultrasound is an ideal and feasible technology to assist enzyme-catalyzed synthesis of designer lipids, and the effect of ultrasound on the structure of enzymes is also worthy of attention.

Tributyrin as a butyric acid precursor has been successfully used for antibacterial effects [20], anticancer [21] and regulation of lipid metabolism [22]. However, tributyrin will be rapidly decomposed into butyric acid and metabolized *in vivo*, which greatly decreases its stability and physiological activity [23,24]. Meanwhile, lauric acid (C12) is a medium-chain fatty acid (MCFA), its glyceride has antibacterial activity and good resistance to digestion, and is rapidly metabolized into energy after being transported to the liver [25]. Therefore, lauric acid may be a potential option to modify tributyrin structure, which improves its nutritional value and stability. In this study, Lipozyme 435 assisted by ultrasonic (28 kHz) synthesized the butyric acid-lauric acid designer lipid (BLDL) for the first time. In particular, the ANN was used to simulate the relationship between butyrate conversion rate and reaction parameters (ultrasonic volume, enzyme loading, substrate molar ratio, reaction temperature and time). On this basis, the optimal parameters combination to achieve the maximum conversion rate of butyric acid was predicted by genetic algorithm (GA). In addition, the structures of Lipozyme 435 with and without ultrasonic treatment were compared. Finally, UPLC-Q-TOF-MS and GC were used to analyze the structure and composition of BLDL. This study is expected to provide innovative ideas for the ultrasound-assisted synthesis of designer lipids, and broaden the application of ANNs in designer lipid synthesis.

2. Materials and methods

2.1. Materials

The reagents purchased from Aladin Co., ltd (Shanghai, China) were listed as follows: lauric acid, tributyrin, butyric acid, glyceryl monobutyrate, glyceryl dibutyrate and lipase from pig pancreas. Lipozyme 435 was purchased from Gaorisen Technology Co., ltd (Beijing, China). All other chemicals used were analytical grade. The trough ultrasonic equipment (JM-03D-28/45) was provided by Shenzhen Jiemeng Technology Co., ltd. (28 kHz, 100 W, 9 s on/6s off). The actual ultrasonic intensity of the device at 100 W power is 1750.1 W/m^2, which was measured by calorimetry [26].

2.2. Ultrasound-assisted BLDL synthesis

2.2.1. Prediction model based on artificial neural network (ANN)

A three-layer feed-forward artificial neural network was used to study the nonlinear relationship between variables (ultrasonic volume, enzyme loading, molar ratio of the substrate, reaction temperature, reaction time) and butyric acid conversion rate. Five variables mentioned above were set as the input layer, while the butyric acid conversion rate was set as the output layer (Fig. 1). Before ANN modeling, a central composite design (CCD, Design Expert 8.0.6) was used to generate 30 experimental runs with ultrasonic volume (11 mL to 16 mL), enzyme loading (8% to 13%, w/w), substrate molar ratio (tributyrin/lauric acid, 0.25 to 0.5), and reaction temperature (55℃ to 70℃) as independent variables and the conversion rate of butyric acid as the dependent variable. The combinations of experimental parameters were shown in Supplementary Table 1. On this basis, each experimental run was sampled by reaction time (0, 30, 60, 120, 180, 240, 360, 480 min), and the raw data for ANN modeling was finally obtained.

In this study, only one hidden layer was selected to prevent over fitting of the model [27]. The training process of the model adopts Marquardt Levenberg learning algorithm, which was a back-propagation training algorithm with high nonlinear mapping ability [28]. In addition, the linear transfer function (*purelin*), log sigmoid transfer function (*logsig*) and hyperbolic tangent sigmoid transfer function (*tansig*) were used for the hidden layer and output layer to obtain the best topology structure of the ANN model for predicting the conversion of tributyrin. The ANN model was constructed by using the "newfit" function in MATLAB, r2009a (the MathWorks, Inc., Ma, USA).

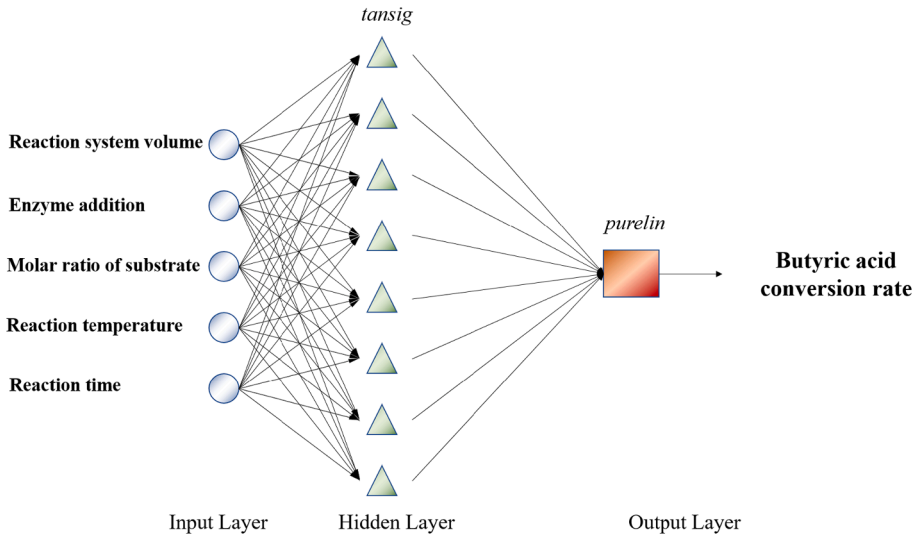

Fig. 1. Architecture of ANN model to predict butyric acid conversion rate as a function of ultrasonic volume, enzyme loading, substrate molar ratio, reaction temperature, and reaction time.

Table 1
Effects of different treatments on secondary structure components of Lipozyme 435 lipase estimated using circular dichroism.

Treatments	α-Helix (%)	β-Sheets (%)	β-Turns (%)	Random coil (%)
Unreacted	71.7	2.3	14.3	11.7
Conventional reaction	5.2	32.2	18.9	43.5
Ultrasound assisted	8.0	35.8	23.9	32.3

Details of modeling could be found in previous studies [27,29].

Finally, the accuracy and predictability of the ANN model were evaluated by coefficient of determination (R^2), root mean square error (RMSE) and absolute mean deviation (AAD). After the ANN model was established, the "slice" function in MATLAB was used to generate a 4D diagram reflecting the effects of ultrasonic volume, enzyme addition, substrate molar ratio, reaction temperature and reaction time on the conversion of tributyrin.

$$R^2 = 1 - \frac{\sum_{i=1}^{n}(q_{i,p} - q_{i,e})^2}{\sum_{i=1}^{n}(q_{i,e} - q_{avg})^2}$$

$$RMSE = \sqrt{\frac{\sum_{i=1}^{n}(q_{i,e} - q_{i,p})^2}{n}}$$

$$ADD = \left[\frac{\sum_{i=1}^{n}\left(\frac{\left|q_{i,p} - q_{i,e}\right|}{q_{i,e}}\right)}{n}\right] * 100$$

In the formulas, $q_{i,p}$ represented the experimental value, $q_{i,e}$ represented the predicted value, q_{avg} meant the average value of the experimental value, and n represented the number of samples.

2.2.2. Optimization based on GA

GA is an adaptive heuristic search and optimization method, which finds the optimal solution by simulating genetics and natural selection [8]. Specifically, each individual with five input variables including the volume of ultrasonication, enzyme loading, molar ratio of the substrate, reaction temperature, and reaction time was defined as chromosome. After these chromosomes were evaluated by adaptability function, the individual with a high fitness score was selected as the parental chromosome. The parental chromosomes repeatedly generated new parental chromosomes and daughter chromosomes through genetic operators such as crossover, mutation and reproduction until the optimal chromosome was obtained, which was the optimal solution [27]. The GA-based optimization process was realized through the optimization toolbox in MATLAB, r2010a (the MathWorks, Inc., Ma, USA).

2.3. Conventional synthesis of BLDL

The stirring-enzyme catalysis method (shaker, 55 rpm) was chosen as the conventional designer lipid synthesis method. The reaction parameters of this protocol were consistent with the best ultrasound assisted lipid synthesis scheme, except that sonication was not added.

2.4. Designer lipid synthesis kinetics

The designer lipid synthesis reaction progress of conventional methods and ultrasound-assisted methods was monitored under optimal reaction conditions. Specifically, samples were taken at 5, 10, 20, 40, 60, 90, and 120 min of the reaction to determine the concentrations of tributyrin and lauric acid.

2.5. Enzyme stability

The stability of Lipozyme 435 was investigated under optimal ultrasound-assisted conditions. Specifically, the enzyme after ultrasound-assisted reaction was collected to washed with *n*-hexane and dried at 40 °C for 60 min. Then, it was cooled in a desiccator for 24 h. Subsequently, the enzyme was used in a second reaction and circulated in this way [30]. The butyric acid conversion rate was determined to assess the stability of enzyme.

2.6. Enzyme activity

2.6.1. Hydrolytic activity of enzyme

Tributyrin (0.02 mol) was mixed with 0.1 g of Lipozyme 435. After 10 min of reaction (56.58 °C), the content of tributyrin was detected through GC (described in section 2.8.1). One unit (U) of Lipozyme 435 hydrolytic activity was defined as the consumption of 1 μmol of tributyrin by 1 mg Lipozyme 435 at 1 min.

2.6.2. Esterification activity of enzyme

Lauric acid (0.02 mol) and 0.02 mol of glycerol were mixed with 0.1 g of Lipozyme 435. After 10 min of reaction (56.58 °C), the content of lauric acid was detected through GC (described in section 2.8.1). One unit (U) of Lipozyme 435 esterification activity was defined as the consumption of 1 μmol of lauric acid by 1 mg Lipozyme 435 at 1 min.

2.7. Structure of enzyme

2.7.1. Circular dichroism (CD)

Enzymes with or without sonication treatment (optimal ultrasonic conditions) were dissolved in 10 mmol/L phosphate buffer (0.3 mg/mL, pH 7.0). The CD (JASCO, J-1500-150ST) was captured in the wavelength range 190–260 nm, with a bandwidth of 1 nm and a scan speed of 100 nm/min, using a 1.0 mm quartz cell. Each spectrum was the average of three consecutive scans and background signal subtracted (phosphate buffer (10 mmol/L, pH 7.0)). The raw data was analyzed on the DichroWeb (http://dichroweb.cryst.bbk.ac.uk/) [31].

2.7.2. Intrinsic fluorescence

The enzymes with or without sonication treatment (optimal ultrasonic conditions) were dissolved in deionized water at a concentration of 0.5 mg/mL. Fluorescence spectra of enzyme samples were measured at room temperature (25 ± 1 °C), using a spectrofluorometer (Model Cary Eclipse, Varian Inc., Palo Alto, USA) equipped with a 1 cm path length cell. The excitation wavelength was 280 nm (slit = 5 nm), the emission wavelength range was 300–400 nm. The voltage applied to the photomultiplier in the detector was 600 V, and the scan speed was 10 nm/s [32].

2.7.3. Fourier transform infrared spectroscopy (FT-IR)

The enzymes with or without sonication treatment (optimal ultrasonic conditions) were freeze-dried to obtain a dry powder (2 mg), which was then pressed into 1–2 mm flakes. Using an FT-IR spectrometer (Thermo Scientific Co., ltd, USA), infrared spectra were recorded by scanning in the 4000–400 cm^{-1} range with 4 cm^{-1} resolution, and 32 scans were performed in each sample.

2.7.4. Scanning electron microscope (SEM)

The microscopic morphology of Lipozyme435 with or without sonication treatment (optimal sonication conditions) was observed by scanning electron microscopy (FEI QUANTA 650). Specifically, the samples were coated with a thin layer of gold for observation with an accelerating voltage of 3–20 kV.

2.7.5. Molecular docking

Molecular docking analysis was performed on tributyrin and lauric acid with Lipozyme 435 lipase, respectively. AutoDockTools (version 1.5.7) software was used for molecular docking studies. According to the research by He et al., the high-resolution (2.60 Å) crystal structure of lipase from *Candida antarctica* (PDB ID: P41365) was downloaded from the Protein Data Bank (PDB) [33]. The PyMOL software (version 2.5.2) was used to remove water and other interfering receptors in the original protein crystal structure to obtain the processed protein crystal. The structures of tributyrin and lauric acid were downloaded from the PubChem website as the SDF files. The minimum energy structures (mol.2 file format) of tributyrin and lauric acid were obtained using Chem3D software. Molecular docking parameters were as follows: adjust the value to cover the active center of the protein, XYZ-dimension was size_x = 90, size_y = 50, size_z = 58, and xyz-center was center_x = 34.018, center_y = 169.501, center_z = 37.134, respectively. The energy range was 5 and the number of runs was 20. Then, the treated protein crystal was docked with tributyrin or lauric acid respectively, the binding mode with the lowest binding energy and the highest binding degree was simulated, and the binding region and site, the active amino acid residues and the main binding force were also obtained. The visualization of molecular docking is realized in PyMOL software.

2.8. Detection of BLDL

2.8.1. Detection of butyric acid conversion rate and lauric acid content

Analysis was performed using a GC-2014 (Shimadzu Co., ltd., Japan) gas chromatography and flame ionization detector (FID). The corresponding conditions were as follows: column: HP-5 (30 m*0.25 mm, inner diameter 0.2um); injection volume: 1 uL; inlet temperature: 310 °C; detector temperature: 320 °C; carrier gas: nitrogen; column pressure: 77 kPa; split ratio: 20:1; heating program: the initial temperature of the column was 50 °C, heated to 260 °C at a rate of 18 °C/min, held for 0.5 min, and then heated to 300 °C at a rate of 20 °C/min. The content (mol) of lauric acid, tributyrin, butyric acid, glyceryl monobutyrate and glyceryl dibutyrate were quantitatively analyzed by standards and standard curve.

$$\text{Butyric acid conversion rate}\,(\%) = \left(1 - \frac{\text{butyric acid}_1 + \text{glyceryl monobutyrate}_1 + \text{glyceryl dibutyrate}_1 * 2 + \text{tributyrin}_1 * 3}{\text{butyric acid}_0 + \text{glyceryl monobutyrat}_0 + \text{glyceryl dibutyrate}_0 * 2 + \text{tributyrin}_0 * 3}\right) * 100$$

In the formulas, 0 indicates content before reaction (mol), 1 indicates content after reaction (mol).

2.8.2. Lipid composition analysis of designer lipid

The designer lipid obtained from the reaction was purified, and the specific purification methods were referred to previous studies [34]. UPLC-Q-TOF-MS (Waters, Milford, MA, USA) was used to analyze triacylglycerol (TAG), diacylglycerol (DAG), monoacylglycerol (MAG) and free fatty acid (FFA) in the designer lipid. Briefly, the UPLC conditions were: BEH C18 (2.1 mm × 150 mm × 1.7 μm, Waters, USA), mobile phase consisted of 90% isopropanol (solvent A), 40% acetonitrile (solvent B), and 10 mmol/L ammonium acetate composition. Lipid was performed at a column temperature of 65 °C with a flow rate of 0.3 mL/min. The gradient program started at 20% A, increased to 75% at 5 min, 90% at 11 min, and then returned to the original 20% at 15 min. The injection volume and concentration were 1 μL and 0.3 mg/mL, respectively.

The Q-TOF-MS was set to positive and negative ion electrospray ionization (ESI) mode. The detailed parameters were described as follows: capillary voltage: 3.5 kV; cone voltage: 20 V; ion source temperature: 100 °C; desolvation temperature: 400 °C; desolvation gas flow rate: 700 L/h; cone gas flow rate: 50 L/h; collision voltage: 6 eV and 30 eV for positive and negative ESI modes, respectively; scan range: 100–1500 *m/z*. Each sample was injected twice, once to detect TAG and MAG in a positive ESI mode and once to detect DAG and FFA in a negative ESI mode. Data processing and analysis using Waters MassLynx software (Waters, Milford, MA, USA) [35].

2.8.3. Analysis of fatty acid composition at sn-2 position

Following the method of Qi et al. with slight modifications, the purified designer lipids were hydrolyzed into *sn*-2 (MAG) using porcine pancreatic lipase in a water bath (37 °C) [36]. The hydrolyzate was

separated on a silica gel plate (G TLC) with the developing solvent of *n*-hexane/diethyl ether/acetic acid (50:50:1, v/v/v). Bands of *sn*-2 MAG were scraped, methylated and analyzed by GC [36].

2.9. Statistical analysis

All experiments were performed at least three times, and the data were expressed as mean ± SD. Prism GraphPad software (version 8.4.0, USA) was used to statistically analyze the data with one-way ANOVA and Turkey test, and $p < 0.05$ was considered as a significant difference.

3. Results

3.1. Establishment of ANN model and parametric study

A three-layer feed-forward ANN model was built to simulate the effects of reaction parameters (ultrasonic volume, enzyme loading, substrate molar ratio, reaction temperature, and reaction time) on butyric acid conversion rate (Fig. 1). The model had an R^2 (0.949) value close to 1, and the RMSE and ADD values were 4.759 and 7.329, respectively (Fig. 2A). Therefore, the ANN model was robust enough to accurately and scientifically fit the relationship functions between reaction parameters and butyric acid conversion rate. Meanwhile, this model could predict the butyric acid conversion rate under specific parameter combinations. In addition, the corresponding weight and bias values of neurons in the hidden and output layers of the model are given in Supplementary Table 2.

Based on ANN and GA tools, the highest predicted conversion rate of butyric acid was obtained, which was 81.39%. In this case, the reaction parameters were combined as follows: treatment volume, enzyme loading, substrate molar ratio (tributyrin: lauric acid), reaction temperature and reaction time were 13.72 mL, 15.49%, 0.253, 56.58℃ and 120 min, respectively. Herein, the experiment with above optimal

Table 2
Lipid composition of BLDL.

TAG	Relative content (%)	DAG	Relative content (%)	FFA	Relative content (%)
La-La-Bu	30.16	La-Bu	4.45	P	1.59
La-La-La	32.12	La-La	20.39	S	1.71
S—O—P	1.54	S—P	2.08	O	0.23
S—O—O	1.10	O—P	2.06		
S—S—O	1.00	S—S	1.30		

La: lauric acid; Bu: butyric acid; S: stearic acid; O: oleic acid; P: Palmitic acid.

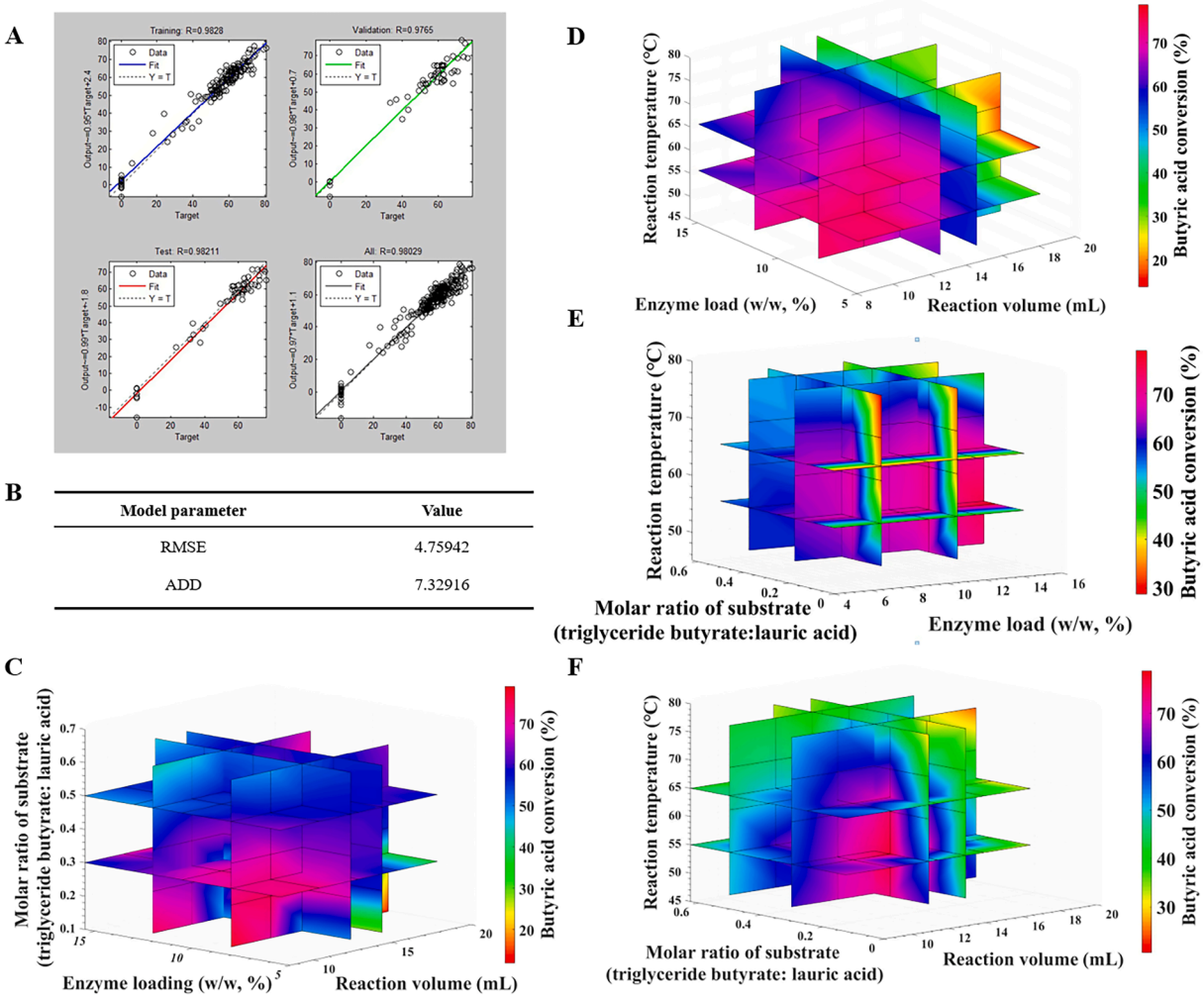

Fig. 2. Predictive accuracy and slice analysis of ANN model. (A, B) Predictive accuracy of ANN model. (C) 4D graph showing the effects of ultrasonic volume, enzyme loading and substrate molar ratio on the adsorption of phenolics on butyric acid conversion rate. (D) 4D graph showing the effects of ultrasonic volume, enzyme loading and reaction temperature on the adsorption of phenolics on butyric acid conversion rate. (E) 4D graph showing the effects of reaction temperature, enzyme loading and substrate molar ratio on the adsorption of phenolics on butyric acid conversion rate. (F) 4D graph showing the effects of reaction temperature, ultrasonic volume and substrate molar ratio on the adsorption of phenolics on butyric acid conversion rate.

parameters combination was performed. The results indicated that the real butyric acid conversion rate was 77.81% which was close to the predicted value. This result further verified the reliability of the established ANN model. Moreover, under the fixed reaction time of 120 min, 4D diagrams of butyric acid conversion rate with independent variables were generated by using slice function (Fig. 2). As shown in Fig. 2C, the promoting effect of ultrasound assistance on the reaction was decreased with the increasing of reaction volume. Additionally, the conversion rate of butyric acid was increased at the molar ratio of substrates (tributyrin/lauric acid) in the range of 0.1–0.3, and started to decrease when the ratio was greater than 0.3. When the molar ratio was greater than 0.5, the impact of enzyme loading and reaction volume on the butyric acid conversion rate was reduced. Interestingly, the results also showed that too high enzyme loading against the synthesis of designer lipid. Combining the results presented in Fig. 2D, E, and F, the thermal inactivation of the enzyme might be the key reason for inhibiting the synthesis of designer lipids when the reaction temperature was higher than 70℃. Furthermore, reaction volume greater than 16 mL were proved to be an unacceptable reaction condition. In all, the ANN is a reliable tool to avoid large tedious experimental operations and improve research efficiency. This study successfully obtained an ANN model, which could well predict and guide the synthesis of BLDL. The optimal parameters combination was used in subsequent experiments, and the optimal butyric acid conversion rate was 77.81%.

3.2. Kinetics of conventional and ultrasound-assisted designer lipid synthesis

As shown in Fig. 3A, 28 kHz ultrasonic assistance significantly increased the butyric acid conversion rate from 69.86% to 77.81%. Notably, the lauric acid content decreased slowly by conventional stirring treated alone, while 28 kHz ultrasound significantly accelerated the consumption of lauric acid, especially in the first 30 min (Fig. 3B). At the end of the reaction, about 20% and 30% of the lauric acid were consumed by conventional stirring and ultrasonic-assisted reaction, respectively. Meanwhile, ultrasound assisted improved the hydrolysis rate of triglyceride. At the end of the reaction, only 6.97% of triglyceride was left, which had a significant downward trend compared with 15.75% in the conventional stirring group (Fig. 3C). Summarily, sonication at 28 kHz distinctly improved the yield of BLDL by increasing the consumption rate and availability of substrates.

3.3. Effect of ultrasound on the stability and vitality of Lipozyme 435

The above results show that BLDL can be successfully obtained by enzymatic catalysis, which should be attributed to the binding of lauric acid and tributyrin to the active site of Lipozyme 435. As shown in Fig. 4A, B, the molecular simulation dockings indicated that the glutamine residue, tryptophan, alanine and isoleucine in the active pocket might be the key site for the reaction of tributyrin and lauric acid catalyzed by Lipozyme 435. In this study, the change of the enzyme activity in the ultrasonic field is an important reason to increase the reaction efficiency. The ultrasonic parameters used in this study (28 kHz, 1750.1 W/m^2, 60% duty cycle, 120 min) did not significantly affect the catalytic synthesis ability of the enzyme within 6 cycles (Fig. 4C). This implied that the effects of ultrasound on enzymes were reversible to some extent. Additionally, it was found that ultrasound dramatically reduced the hydrolysis activity of Lipozyme 435 ($p < 0.01$), while enhancing the esterification activity of the enzyme ($p < 0.05$) (Fig. 4 D, E). This was contrary to the phenomenon that ultrasound enhanced the consumption of tributyrin and lauric acid (Fig. 3B, C). It was suggested that ultrasonic treatment may stimulate acidolysis transesterification through multiple pathways. Due to the changes in the enzyme activity by ultrasonic treatment, the related indexes of the enzyme structure

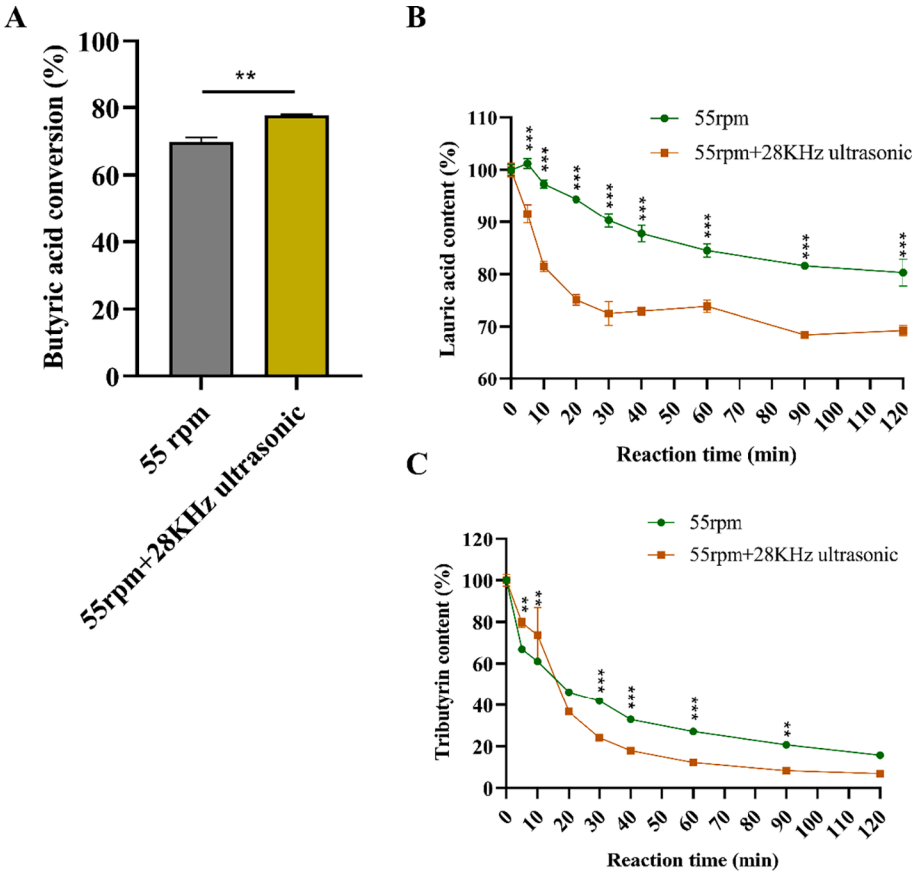

Fig. 3. Comparison of conventional and ultrasound-assisted designer lipid synthesis. (A) Butyric acid conversion rates of conventional (55 rpm) and ultrasound-assisted (55 rpm + 28 kHz ultrasonic) designer lipid synthesis. (B) Lauric acid content during conventional (55 rpm) and ultrasound-assisted (55 rpm + 28 kHz ultrasonic) synthesis. Significant difference markers indicated that there were significant differences between different treatment groups. (C) Tributyrin content during conventional (55 rpm) and ultrasound-assisted (55 rpm + 28 kHz ultrasonic) synthesis. Significant difference markers indicated that there were significant differences between different treatment groups. ** indicated significant differences ($p < 0.01$), *** indicated extremely significant differences ($p < 0.001$).

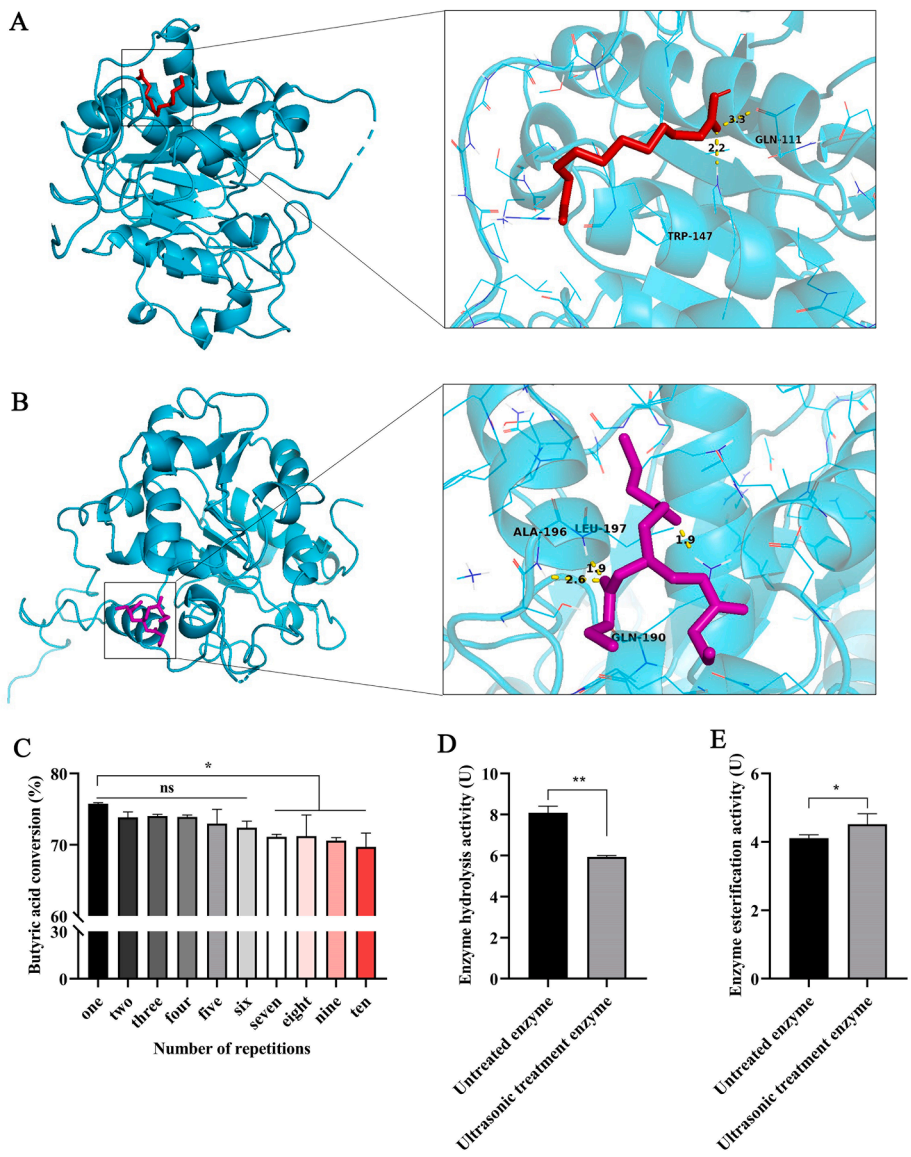

Fig. 4. Effect of ultrasound on the stability and vitality of Lipozyme 435. (A) The molecular docking between lauric acid and un-ultrasonic treatment *Candida antarctica* lipase B (Lipozyme 435), the yellow dashed line represented the simulated hydrogen bond connection, and the number indicated the hydrogen bond distance (Å). (B) The molecular docking between tributyrin and un-ultrasonic treatment *Candida antarctica* lipase B (Lipozyme 435), the yellow dashed line represented the simulated hydrogen bond connection, and the number indicated the hydrogen bond distance (Å). (C) Stability of Lipozyme 435 assisted by ultrasound. (D) Hydrolysis activity of Lipozyme 435 after conventional and ultrasonic treatment. (E) Esterification activity of Lipozyme 435 after conventional and ultrasonic treatment. * indicated significant differences ($p < 0.05$), ** indicated $p < 0.01$. (For interpretation of the references to color in this figure legend, the reader is referred to the web version of this article.)

were further monitored below.

3.4. The effect of ultrasound on the structure of Lipozyme 435

3.4.1. FT-IR spectrum analysis

FT-IR spectroscopy was used to determine the structural changes of Lipozyme 435 before and after ultrasonic treatment (Fig. 5A). Compared with the unreacted enzyme, both the 3420 cm^{-1} and the 2950 cm^{-1} positions of the conventional reaction enzyme and ultrasonic treatment enzyme were shifted to lower wavenumbers. These peaks were generated by the O—H stretching vibration and the C—H stretching vibration respectively, which implied that the enzyme-catalyzed reaction may lead to partial hydrogen bond formation. In addition, the amide structure is an important structure in proteins. According to the wavenumber range, amides can be divided into amide I (1700–1600 cm^{-1}), amide II (1550–1530 cm^{-1}) and amide III (1300–1260 cm^{-1}). In the amide I region, the waveforms of the conventional reaction enzyme and ultrasonic treatment enzyme changed greatly (1730 cm^{-1}) and the peak in the 1650 cm^{-1} region became flat. This change might be reversed by washing with *n*-hexane after the reaction. Compared with conventional reactive enzyme, ultrasonic treatment sharpened the shape of the enzyme peak at 1730 cm^{-1}. In amide II region, Lipozyme 435 after reaction had no obvious peak. Fig. 5A also showed that after catalytic reaction, the peak shape in 1300–1200 cm^{-1} band was slightly changed, which still occurred after *n*-hexane washing.

3.4.2. Intrinsic fluorescence analysis

Disruption of the protein structure results in the exposure of tryptophan residues, which is ultimately revealed in fluorescent properties. In this study, intrinsic fluorescence was used to observe the effect of sonication on Lipozyme 435. As shown in Fig. 5B, the maximum fluorescence emission wavelength of unreacted Lipozyme 435 was 326 nm with an intensity of 632.5 a.u.. Compared with the unreacted Lipozyme 435, the maximum fluorescence emission wavelength of the reacted ones showed an obvious red-shift phenomenon and its fluorescence intensity decreased sharply. Specifically, the maximum fluorescence emission wavelengths of Lipozyme 435 after the conventional and sonication reaction were shifted to 357 nm and 346 nm, respectively (Fig. 5C). Besides, the maximum fluorescence intensity of the enzyme after ultrasonic-assisted reaction was significantly reduced compared with the conventional reaction group. These results implied that sonication caused unfolding of the tertiary structure of lipase, changing the spatial position of tryptophan residues. However, the red-shift of the maximum fluorescence emission wavelength might be due to the

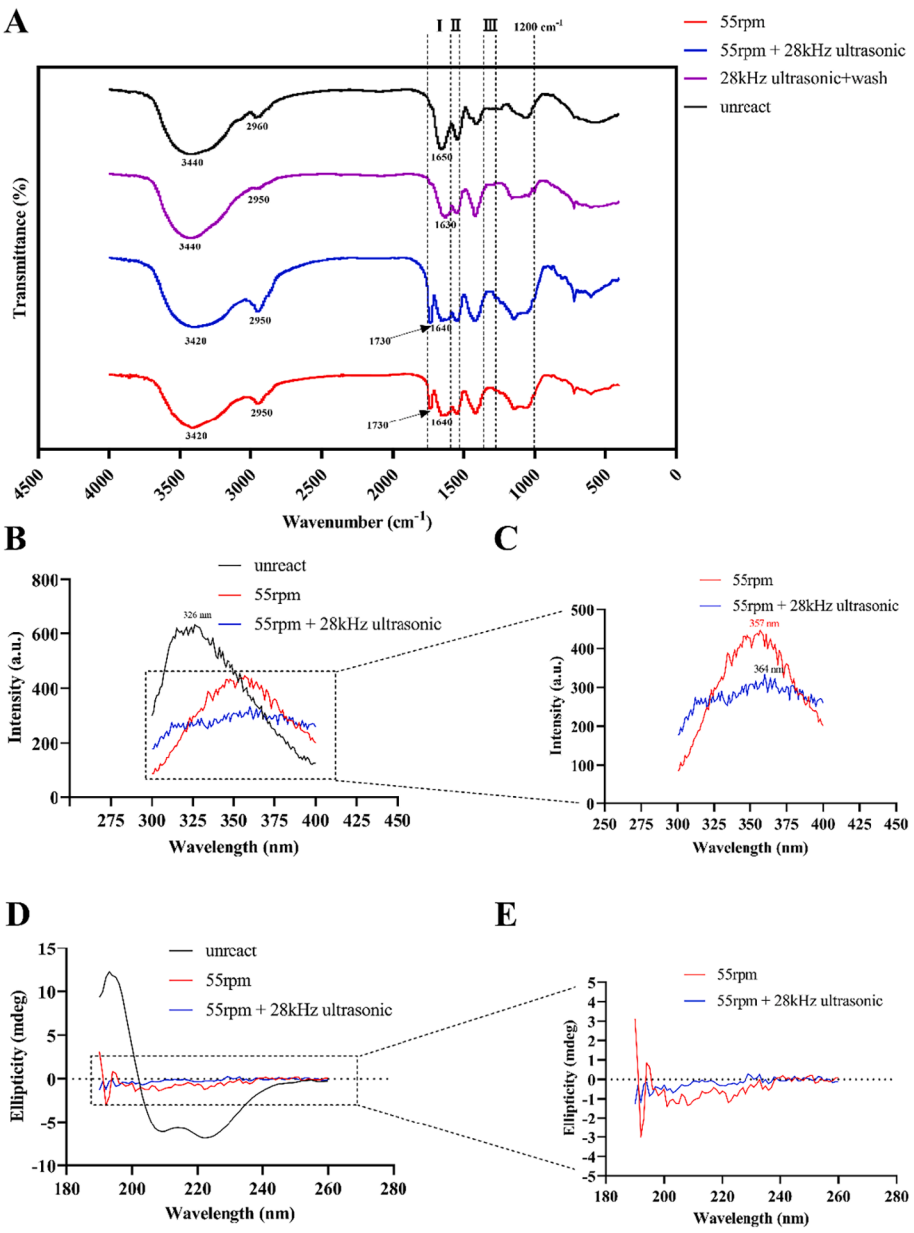

Fig. 5. The effect of ultrasound on the structure of Lipozyme 435. (A) FT-IR spectrum analysis. (B) Intrinsic fluorescence of unreacted (unreact), conventionally reacted (55 rpm), and ultrasound-assisted reacted (55 rpm + 28 kHz ultrasonic) Lipozyme 435. (C) Intrinsic fluorescence of conventionally reacted (55 rpm) and ultrasound-assisted reacted (55 rpm + 28 kHz ultrasonic) Lipozyme 435. (D) Circular dichroism of unreacted (unreact), conventionally reacted (55 rpm), and ultrasound-assisted reacted (55 rpm + 28 kHz ultrasonic) Lipozyme 435. (E) Circular dichroism of conventionally reacted (55 rpm) and ultrasound-assisted reacted (55 rpm + 28 kHz ultrasonic) Lipozyme 435.

heating.

3.4.3. Circular dichroism analysis

The secondary structure of the reacted lipase changed obviously (Fig. 5 D, E; Table 1). In unreacted Lipozyme 435, the α-Helix structure occupied 71.7%, accompanied with 2.3% β-Sheets, 14.3% β-Turns and 14.4% random coil (Table.1). It was worth noting that the effect of heating as well as ultrasound on the secondary structure of lipase was strong. The α-Helix of the enzyme decreased after the reaction, and the β-Sheets of enzymes in the conventional treatment and ultrasound groups contained 32.2% and 35.8%, respectively, which were increased after reaction. Meanwhile, the β-Turns also increased from 14.3% before the reaction to 18.9% after the conventional reaction and 23.9% after sonication. In addition, a dramatic increase in the proportion of random coils was also observed after the reaction. Compared with the conventional treatment, the ultrasonic treatment transformed less α-Helix into random coil, and its content was 11.2% lower than that of the conventional treatment group.

3.4.4. Microstructure of Lipozyme 435

The effect of ultrasonic treatment on Lipozyme 435 microstructure was observed by SEM (Fig. 6). The Lipozyme 435 without ultrasonic treatment presented the original smooth and dense spherical structure of the carrier resin. However, ultrasound at 28 kHz resulted in fractures and voids on the surface of the immobilized carrier, and even irregular deformation of the spherical structure. Those larger voids in the encapsulating material of the immobilized enzyme contribute to facilitating the binding of substrate and enzyme. In addition, conventional treatment (56.5 °C, 55 rpm) did not cause significant changes in the surface structure of Lipozyme 435.

3.5. Lipid composition and sn-2 fatty acid of BLDL

In this study, the lipid composition of BLDL was analyzed using UPLC-Q-TOF-MS. As shown in Table. 2, the BLDL contained 34.61% of butyric lauric acid structural lipids (including La-La-Bu and La-Bu). Moreover, glyceryl trilaurate and glyceryl dilaurate were the main reaction by-products, accounting for 32.12% and 20.39%, respectively.

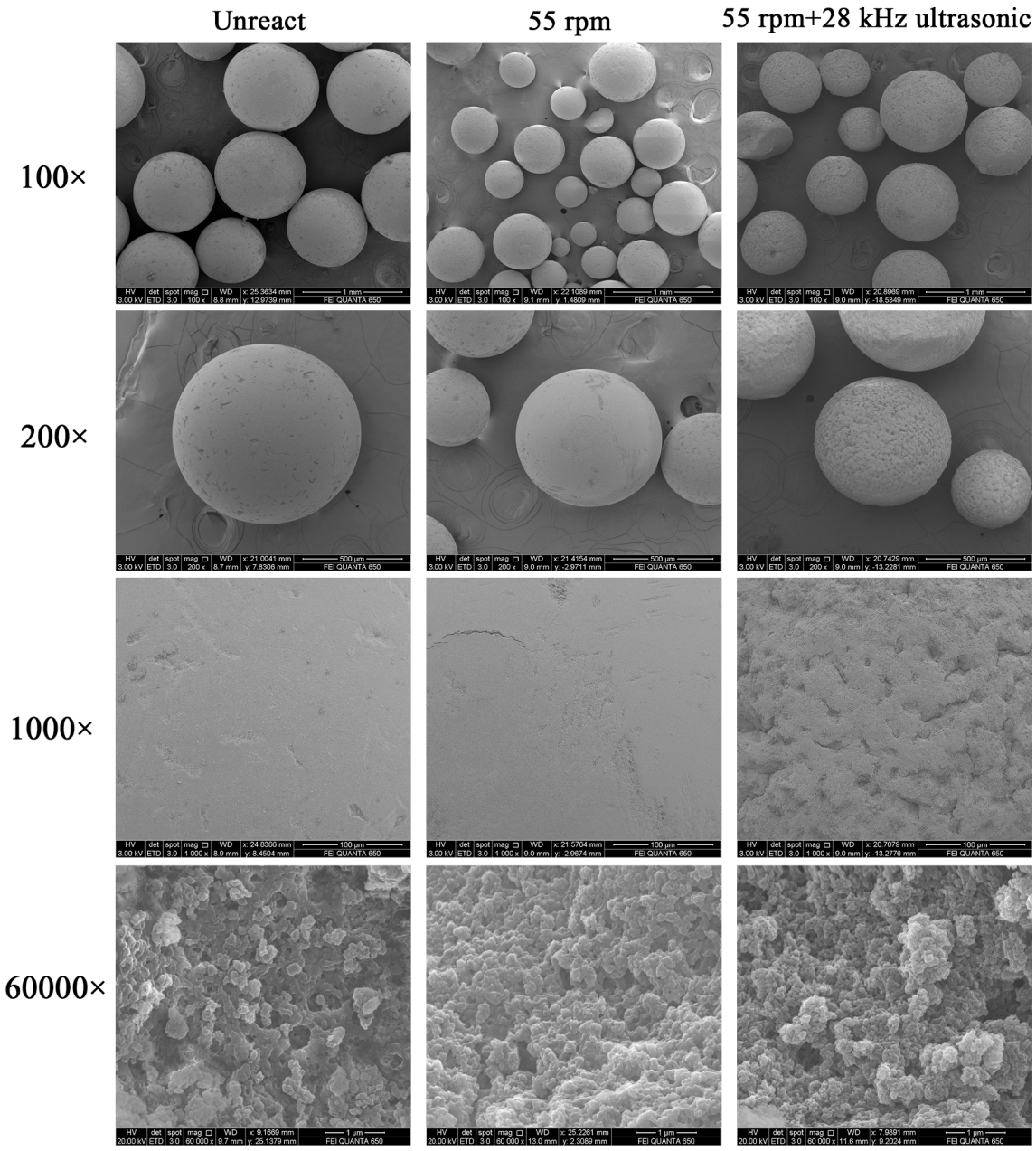

Fig. 6. Scanning electron microscopic photograph of Lipozyme 435 (with different treatment).

Small amounts of free or esterified stearic acid, oleic acid, and palmitic acid were also detected. On the other hand, lauric acid was the main fatty acid distributed in the *sn*-2 position of the glycerol backbone of purified BLDL, accounting for about 96.2%. In conclusion, ultrasound-assisted Lipozyme 435 catalyzed acid hydrolysis and trans-esterification, successfully synthesizing objective butyric lauric acid structural lipids.

4. Discussion

In this study, ultrasound was used for the first time to enhance Lipozyme 435 catalyzed synthesis of BLDL, whose treatment condition was optimized guided by the ANN model. ANN model is an evolutionary computational model. Compared with the response surface, which only considers the quadratic nonlinear correlation between factors, ANN can combine multiple dependent variables and independent variables together to more accurately solve complex nonlinear system identification and control problems [7,37]. This study established an ANN reflecting the effects of independent variables (ultrasonic volume, enzyme loading, substrate molar ratio, reaction temperature, and reaction time) on the butyric acid conversion. The model contained only one hidden layer and reached a comfortable accuracy after training (R^2 = 0.949, RMSE = 4.759, ADD = 7.329). The optimized synthesis protocol of the ANN established in this study was an ultrasonic reaction volume of 13.72 mL, an enzyme loading of 15.49%, a substrate molar ratio of 0.253, a reaction temperature of 56.58 °C, and reaction time of 120 min. The BLDL synthesized under this scheme contains 30.16% La-La-Bu and 4.45% La-Bu, and the main fatty acids distributed at the *sn*-2 position were butyric acid and lauric acid, containing 3.8% and 96.2%, respectively. Similarly, Esonye et al. optimized biodiesel production from sweet almond (*Prunus amygdalus*) seed oil using a response surface approach and ANN [7]. In their study, ANN showed strong prediction and fitting ability (R = 0.9663), and finally obtained the optimal synthesis scheme was catalyst concentration of 1.5 (w/w%), reaction time

of 65 min, oil/methanol molar ratio of 1:5 and 50 ℃ reaction temperature. In this research, ultrasound-assisted treatment (28 kHz, 100 W, 120 min, 60% duty cycle) significantly improved the BLDL yield (Fig. 3), from 69.86% of conventional reaction to 77.81%. This phenomenon may be related to the turbulent flow caused by the cavitation phenomenon of ultrasound in the liquid medium, which accelerates the mass transfer process of the material [1]. Consistently, slice analysis found that the decrease in ultrasonic energy density caused by the increase of ultrasonic reaction volume may further lead to the decrease in butyric acid conversion rate (Fig. 2) [38]. Moreover, the consumption rate and degree of tributyrin and lauric acid under ultrasonic assistance were higher than those of the conventional treatment group. Previously, ultrasound in the frequency range of 20 kHz-100 kHz was also reported to enhance mass transfer and enzyme catalysis [39,40]. Jadhav et al. used a 22 kHz, 240 W, 50% duty cycle ultrasonic probe to enhance the synthesis of medium-chain fatty acid designer lipids with linseed oil, caprylic acid, and capric acid [41]. They reported that sonication increased designer lipid yields from<20% for conventional reactions to 96% within 90 min, demonstrating the intensification advantage of the sonication-assisted method. In 2021, this team also revealed the positive effect of ultrasound assistance (20 kHz, 240 W, 70% duty cycle, 360 min action time) in improving the efficiency of the acid hydrolysis reaction between palm olein and caprylic acid, and obtained designer lipids with stronger oxidative stability [3]. Additionally, our study found that under the ultrasonic conditions of 28 kHz, 100 W, 56.5℃ and 60% duty cycle for 120 min, the lauric acid esterification activity of lipozyme 435 could be significantly improved ($p < 0.05$), and its hydrolysis activity to triglyceride was significantly reduced ($p < 0.01$). The vibration and collapse of bubbles caused by ultrasound in the medium may lead to the destruction of hydrogen bonds and van der Waals force in protein molecules, and then the partial dissociation of enzyme structure and the positive or negative changes of enzyme activity [42]. However, the changes in enzymatic activity by sonication appear to be reversible to a certain extent. In this study, it was found that Lipozyme 435 could be recycle stably for 6 times in an ultrasound condition.

In addition to facilitate the contact between the enzyme and substrate, direct stimulation of enzyme activity by ultrasound is also a potential mechanism [43]. The structural changes of the enzymes induced by ultrasound might ultimately mediate the changes in enzyme activity. FT-IR can display the position and intensity changes of protein amide I band, amide II band and amide III band, providing information on the secondary structure of the peptide chain. According to the FT-IR results, the amide I band (1700–1600 cm^{-1}) of the reacted Lipozyme 435 moved to around 1700 cm^{-1} relative to the unreacted enzyme. In particular, the ultrasonic treatment group showed a stronger amide I band signal than the conventional reaction group (Fig. 5). The amide I band was reported to correspond to the side chain uptake of glutamine, asparagine, and arginine. Thus, sonication assistance exposed more asparagine, arginine, glutamine, and glutamate residues, which might be related to the strong shear force and partial high temperature generated by the ultrasonic-induced collapse of cavitation bubbles [43,44]. Glutamine is an important amino acid residue in the active pocket of Lipozyme 435 (Fig. 4A, B). The changes of enzyme activity caused by ultrasound may be related to the spatial position changes of glutamine residues. Furthermore, CD is a non-destructive tool for monitoring protein conformational changes, which was used to identify the effect of sonication on the ratio of α-helix, β-sheet, β-turn and random coil structure of Lipozyme 435. The results showed that heating and ultrasound significantly reduced the ratio of α-helix, and ultrasound treatment more violently increased the proportion of β-turn and β-sheets compared with conventional treatment. A similar phenomenon was also reported by Wang et al., who found that the α-helical structure of free cellulase was partially deformed and the random coil content increased after 10 min of low-intensity sonication dispose at 15 W, 24 kHz [45]. These changes may be caused by mechanical shearing and local transient heating in the duration of ultrasound. Admittedly, ultrasound-mediated changes in protein conformation are multidirectional. Another study indicated that sonication was able to increase α-helix and random coil content and lead to loss of β-sheets [46]. Moreover, intrinsic fluorescence was used to explore ultrasound-induced changes in the tertiary structure of the enzyme. The result presented that the maximum fluorescence emission wavelength of Lipozyme 435 after the reaction (both conventional and ultrasonic treatment) showed an obvious red-shift phenomenon, and its fluorescence intensity also dropped sharply. Among them, the fluorescence intensity of the ultrasonic treatment group was lower than that of the conventional treatment group (Fig. 5). The intrinsic fluorescence of proteins is mainly contributed by tryptophan, tyrosine and phenylalanine residues, especially tryptophan residues. The decrease of fluorescence intensity may be related to the mechanical and thermal effects of ultrasound. These effects induce protein conformational changes and lead to the exposure of more hydrophobic groups inside the molecule to the outside, covering the original tryptophan residues on the protein surface [42]. Similar results were also reported by Ma et al. [47] and Wang et al. [45]. These ultrasonic-induced changes in the enzyme structure may lead to expose internal active pocket of the enzyme, making it easier for the substrate to contact the active site, and ultimately improve the catalytic activity of the enzyme. Besides, sonication significantly changed the surface morphology of the immobilized enzyme particles (Fig. 6). Mechanical shear, shock waves, and turbulence introduced by ultrasonic waves could lead to more voids and fractures on the surface of the fixed substrate [48]. To a certain extent, this slight destructive effect can increase the specific surface area of the immobilized enzyme and accelerate the reaction. However, the mechanism of the differential effects of ultrasound on the esterification hydrolysis activity of Lipozyme 435 requires further investigation.

5. Conclusion

Ultrasound-assisted treatment significantly improved the BLDL yield up to 77.81%, and the purified BLDL contained about 34.61% of butyric acid-lauric acid structural lipids. Meanwhile, the optimal reaction of parameters predicted by ANN was as follows: reaction volume, enzyme load, substrate molar ratio (tributyrin/lauric acid), reaction temperature and reaction time were 13.72 mL, 15.49%, 0.253, 56.58 °C and 120 min, respectively. With ultrasonic treatment, the secondary structures of the enzyme were altered, such as the vibrational change of the amide I band, the decrease of α-helix, the increase of β-sheet and β-turn content. The ultrasonic treatment also increased the cracks and voids on the surface of the immobilized support. Moreover, the change in enzyme structure could be partially reversed by *n*-hexane, and the enzyme synthesis activity showed stability within 6 reaction cycles.

CRediT authorship contribution statement

Wangxin Liu: Conceptualization, Data curation, Formal analysis, Investigation, Writing – original draft, Writing – review & editing. **Xianliang Luo:** Conceptualization, Data curation, Formal analysis, Investigation, Writing – review & editing. **Yang Tao:** Formal analysis, Conceptualization, Writing – review & editing. **Ying Huang:** Formal analysis, Investigation, Writing – review & editing. **Minjie Zhao:** Formal analysis, Investigation, Writing – review & editing. **Jiahui Yu:** Data curation, Writing – review & editing. **Fengqin Feng:** Conceptualization, Supervision, Project administration, Funding acquisition, Writing – review & editing. **Wei Wei:** Conceptualization, Supervision, Project administration, Writing – review & editing.

Declaration of Competing Interest

The authors declare that they have no known competing financial interests or personal relationships that could have appeared to influence the work reported in this paper.

Acknowledgements

Thanks to Guangjie Xie for his help in experimental design. This research was supported by Key Project of Natural Science Foundation of Zhejiang Province (Grant No.LD19C200001), and the National Natural Science Foundation of China (32072224).

Appendix A. Supplementary data

Supplementary data to this article can be found online at https://doi.org/10.1016/j.ultsonch.2022.106100.

References

[1] H.B. Jadhav, U. Annapure, Designer lipids -synthesis and application-A review, Trends Food Sci. Tech. 116 (2021) 884–902, https://doi.org/10.1016/j.tifs.2021.08.020.
[2] W. Wei, Y.F. Feng, X. Zhang, X. Ca, F.Q. Feng, Synthesis of structured lipid 1,3-dioleoyl-2-palmitoylglycerol in both solvent and solvent-free system, LWT-Food Sci. Technol. 60 (2015) 1187–1194, https://doi.org/10.1016/j.lwt.2014.09.013.
[3] H.B. Jadhav, P.R. Gogate, J.T. Waghmare, U.S. Annapure, Intensified synthesis of palm olein designer lipids using sonication, Ultrason. Sonochem. 73 (2021), 105478, https://doi.org/10.1016/j.ultsonch.2021.105478.
[4] H.L. Mu, J.P. Kurvinen, H. Kallio, X.B. Xu, C.E. Hoy, Quantitation of acyl migration during lipase-catalyzed acidolysis, and of the regioisomers of structured triacylglycerols formed, J. Am. Oil Chem. Soc. 78 (2001) 959–964, https://doi.org/10.1007/s11746-001-0371-3.
[5] M. Szczesna-Antczak, A. Kubiak, T. Antczak, S. Bielecki, Enzymatic biodiesel synthesis - Key factors affecting efficiency of the process, Renew Energ. 34 (2009) 1185–1194, https://doi.org/10.1016/j.renene.2008.11.013.
[6] T.L. Yuan, W. Wei, X.G. Wang, Q.Z. Jin, Biosynthesis of structured lipids enriched with medium and long-chain triacylglycerols for human milk fat substitute, LWT-Food Sci. Technol. 128 (2020), 109255, https://doi.org/10.1016/j.lwt.2020.109255.
[7] C. Esonye, O.D. Onukwuli, A.U. Ofoefule, Optimization of methyl ester production from Prunus Amygdalus seed oil using response surface methodology and Artificial Neural Networks, Renew Energy 130 (2019) 61–72, https://doi.org/10.1016/j.renene.2018.06.036.
[8] K.M. Desai, S.A. Survase, P.S. Saudagar, S.S. Lele, R.S. Singhal, Comparison of artificial neural network (ANN) and response surface methodology (RSM) in fermentation media optimization: Case study of fermentative production of scleroglucan, Biochem. Eng. J. 41 (2008) 266–273, https://doi.org/10.1016/j.bej.2008.05.009.
[9] R. Foroutan, R. Mohammadi, J. Razeghi, B. Ramavandi, Biodiesel production from edible oils using algal biochar/CaO/K2CO3 as a heterogeneous and recyclable catalyst, Renew. Energy 168 (2021) 1207–1216, https://doi.org/10.1016/j.renene.2020.12.094.
[10] S.Y. Zhang, S.A. Willett, J.R. Hyatt, S. Martini, C.C. Akoh, Phenolic compounds as antioxidants to improve oxidative stability of menhaden oil-based structured lipid as butterfat analog, Food Chem. 334 (2021), 127584, https://doi.org/10.1016/j.foodchem.2020.127584.
[11] J.Y. Lu, Q.Z. Jin, X.G. Wang, X.S. Wang, Preparation of medium and long chain triacylglycerols by lipase-catalyzed interesterification in a solvent-free system, Process Biochem. 54 (2017) 89–95, https://doi.org/10.1016/j.procbio.2016.12.015.
[12] T.K. Yang, M.B. Fruekilde, X.B. Xu, Suppression of acyl migration in enzymatic production of structured lipids through temperature programming, Food Chem. 92 (2005) 101–107, https://doi.org/10.1016/j.foodchem.2004.07.007.
[13] Fazlena H, Norsuraya S, Nadiah SN. Ultrasonic Assisted Enzymatic Reaction: An Overview on Ultrasonic Mechanism and Stability-Activity of the Enzyme. 2013 IEEE Business Engineering and Industrial Applications Colloquium (BEIAC 2013). 2013:85-90.
[14] B. Condon, M. Easson, V. Yachmenev, A. Lambert, J. Smith, Application of low level, uniform ultrasound field for acceleration of enzymatic bio-processing of cotton, Cellul. Chem. Technol. 43 (2009) 929–942, https://doi.org/10.1007/s10570-009-9336-7.
[15] K.S. Suslick, N.C. Eddingsaas, D.J. Flannigan, S.D. Hopkins, H. Xu, Extreme conditions during multibubble cavitation: Sonoluminescence as a spectroscopic probe, Ultrason. Sonochem. 18 (2011) 842–846, https://doi.org/10.1016/j.ultsonch.2010.12.012.
[16] S.L. Liu, X.Y. Dong, F. Wei, X. Wang, X. Lv, J. Zhong, et al., Ultrasonic pretreatment in lipase-catalyzed synthesis of structured lipids with high 1,3-dioleoyl-2-palmitoylglycerol content, Ultrason. Sonochem. 23 (2015) 100–108, https://doi.org/10.1016/j.ultsonch.2014.10.015.
[17] S.B. More, P.R. Gogate, J.S. Waghmare, S.N. Naik, Intensified synthesis of structured triacylglycerols from fish, flaxseed and rice bran oil using supercritical CO2 or ultrasound, Chem. Eng. Process. Process Intensif. 144 (2019), 107650, https://doi.org/10.1016/j.cep.2019.107650.
[18] E. Joyce, S.S. Phull, J.P. Lorimer, T.J. Mason, The development and evaluation of ultrasound for the treatment of bacterial suspensions. A study of frequency, power and sonication time on cultured Bacillus species, Ultrason. Sonochem. 10 (2003) 315–318, https://doi.org/10.1016/S1350-4177(03)00101-9.
[19] Q.A. Zhang, Y.Y. Yan, X.H. Fan, X.L. Zhang, Effects of Ultrasound Working Parameters on the Ultrasonic Power Density Some Neglected Problems in the Application of Ultrasound Bath, Iran J. Chem. Chem. Eng. 36 (2017) 161–171, https://doi.org/10.30492/IJCCE.2017.28074.
[20] H. Namkung, H. Yu, J. Gong, S. Leeson, Antimicrobial activity of butyrate glycerides toward Salmonella Typhimurium and Clostridium perfringens, Poult. Sci. 90 (2011) 2217–2222, https://doi.org/10.3382/ps.2011-01498.
[21] M.J. Edelman, K. Bauer, S. Khanwani, N. Tait, J. Trepel, J. Karp, et al., Clinical and pharmacologic study of tributyrin: an oral butyrate prodrug, Cancer Chemother. Pharmacol. 51 (2003) 439–444, https://doi.org/10.1007/s00280-003-0580-5.
[22] F. Yin, H. Yu, D. Lepp, X. Shi, X. Yang, J. Hu, et al., Transcriptome Analysis Reveals Regulation of Gene Expression for Lipid Catabolism in Young Broilers by Butyrate Glycerides, PLoS One 11 (2016) e0160751.
[23] S. Molina, M.I. Moran-Valero, D. Martin, L. Vazquez, T. Vargas, C.F. Torres, et al., Antiproliferative effect of alkylglycerols as vehicles of butyric acid on colon cancer cells, Chem. Phys. Lipids 175 (2013) 50–56, https://doi.org/10.1016/j.chemphyslip.2013.07.011.
[24] W. Liu, X. Luo, J. Wang, Y. Li, F. Feng, M. Zhao, Digestive behavior of unemulsified triglycerides with different chain lengths: In vitro dynamic and static simulated digestion models, LWT. 149 (2021), 112006, https://doi.org/10.1016/j.lwt.2021.112006.
[25] F.M. Dayrit, The Properties of Lauric Acid and Their Significance in Coconut Oil, J. Am. Oil Chem. Soc. 92 (2015) 1–15, https://doi.org/10.1007/s11746-014-2562-7.
[26] H. Kiani, D.W. Sun, Z.H. Zhang, The effect of ultrasound irradiation on the convective heat transfer rate during immersion cooling of a stationary sphere, Ultrason. Sonochem. 19 (2012) 1238–1245, https://doi.org/10.1016/j.ultsonch.2012.04.009.
[27] Y. Tao, D. Wu, Q.A. Zhang, D.W. Sun, Ultrasound-assisted extraction of phenolics from wine lees: Modeling, optimization and stability of extracts during storage, Ultrason. Sonochem. 21 (2014) 706–715, https://doi.org/10.1016/j.ultsonch.2013.09.005.
[28] D. Wu, J.Y. Chen, B.Y. Lu, L.N. Xiong, Y. He, Y. Zhang, Application of near infrared spectroscopy for the rapid determination of antioxidant activity of bamboo leaf extract, Food Chem. 135 (2012) 2147–2156, https://doi.org/10.1016/j.foodchem.2012.07.011.
[29] Y. Tao, Y.B. Han, W.X. Liu, L. Peng, Y. Wang, S. Kadam, et al., Parametric and phenomenological studies about ultrasound-enhanced biosorption of phenolics from fruit pomace extract by waste yeast, Ultrason. Sonochem. 52 (2019) 193–204, https://doi.org/10.1016/j.ultsonch.2018.11.018.
[30] A. Galgali, S.D. Gawas, V.K. Rathod, Ultrasound assisted synthesis of citronellol laurate by using Novozym 435, Catal. Today 309 (2018) 133–139, https://doi.org/10.1016/j.cattod.2017.08.052.
[31] F. Wang, Y.Z. Zhang, L. Xu, H. Ma, An efficient ultrasound-assisted extraction method of pea protein and its effect on protein functional properties and biological activities, Lwt-Food Sci. Technol. 127 (2020), 109348, https://doi.org/10.1016/j.lwt.2020.109348.
[32] B.G. Xu, J. Yuan, L. Wang, F. Lu, B.X. Wei, R.S.M. Azam, et al., Effect of multi-frequency power ultrasound (MFPU) treatment on enzyme hydrolysis of casein, Ultrason. Sonochem. 63 (2020), 104930, https://doi.org/10.1016/j.ultsonch.2019.104930.
[33] Y.J. He, C.Y. Qiu, Z. Guo, J. Huang, M.Z. Wang, B.L. Chen, Production of new human milk fat substitutes by enzymatic acidolysis of microalgae oils from Nannochloropsis oculata and Isochrysis galbana, Bioresour. Technol. 238 (2017) 129–138, https://doi.org/10.1016/j.biortech.2017.04.041.
[34] W. Liu, X. Luo, T. Liu, F. Feng, Study on the digestive characteristics of short-and medium-chain fatty acid structural lipid and its rapid intervention on gut microbes: In vivo and in vitro studies, Food Chem. 380 (2022), 131792, https://doi.org/10.1016/j.foodchem.2021.131792.
[35] L. Wang, X. Zhang, T. Yuan, Q. Jin, W. Wei, X. Wang, Digestion of Medium- and Long-Chain Triacylglycerol and sn-2 Palmitate in Infant Formula: A Study Based on Dynamic In Vitro Simulation of Infant Gastrointestinal Lipolysis, J. Agric. Food Chem. 70 (2022) 3263–3271, https://doi.org/10.1021/acs.jafc.1c07118.
[36] C. Qi, J. Sun, Y. Xia, R.Q. Yu, W. Wei, J.Y. Xiang, et al., Fatty Acid Profile and the sn-2 Position Distribution in Triacylglycerols of Breast Milk during Different Lactation Stages, J. Agric. Food Chem. 66 (2018) 3118–3126, https://doi.org/10.1021/acs.jafc.8b01085.
[37] F. Geyikci, E. Kilic, S. Coruh, S. Elevli, Modelling of lead adsorption from industrial sludge leachate on red mud by using RSM and ANN, Chem. Eng. J. 183 (2012) 53–59, https://doi.org/10.1016/j.cej.2011.12.019.
[38] C.P. O'Donnell, B.K. Tiwari, P. Bourke, P.J. Cullen, Effect of ultrasonic processing on food enzymes of industrial importance, Trends Food Sci. Technol. 21 (2010) 358–367, https://doi.org/10.1016/j.tifs.2010.04.007.
[39] Y. Tao, Y. Wu, Y.B. Han, F. Chemat, D.D. Li, P.L. Show, Insight into mass transfer during ultrasound-enhanced adsorption/desorption of blueberry anthocyanins on macroporous resins by numerical simulation considering ultrasonic influence on resin properties, Chem. Eng. J. 380 (2020), https://doi.org/10.1016/j.cej.2019.122530.
[40] Y. Tao, P.F. Wu, Y.X. Dai, X.T. Luo, S. Manickam, D.D. Li, et al., Bridge between mass transfer behavior and properties of bubbles under two-stage ultrasound-assisted physisorption of polyphenols using macroporous resin, Chem. Eng. J. 436 (2022), https://doi.org/10.1016/j.cej.2022.135158.
[41] H.B. Jadhav, P. Gogate, U. Annapure, Process intensification of acidolysis reaction catalysed by enzymes for synthesis of designer lipids using sonication, Chem. Eng. J. 428 (2022), 131374, https://doi.org/10.1016/j.cej.2021.131374.

[42] A. Cordova, P. Henriquez, H. Nunez, F. Rico-Rodriguez, C. Guerrero, C. Astudillo-Castro, et al., Recent Advances in the Application of Enzyme Processing Assisted by Ultrasound in Agri-Foods: A Review, Catalysts 12 (2022) 107, https://doi.org/10.3390/catal12010107.

[43] S.S. Nadar, V.K. Rathod, Sonochemical Effect on Activity and Conformation of Commercial Lipases, Appl. Biochem. Biotechnol. 181 (2017) 1435–1453, https://doi.org/10.1007/s12010-016-2294-2.

[44] Z.L. Yu, W.C. Zeng, X.L. Lu, Influence of ultrasound to the activity of tyrosinase, Ultrason. Sonochem. 20 (2013) 805–809, https://doi.org/10.1016/j.ultsonch.2012.11.006.

[45] Z.B. Wang, X.M. Lin, P.P. Li, J. Zhang, S.Q. Wang, H.L. Ma, Effects of low intensity ultrasound on cellulase pretreatment, Bioresour. Technol. 117 (2012) 222–227, https://doi.org/10.1016/j.biortech.2012.04.015.

[46] L.R. Huang, W.X. Zhang, X.N. Ding, Z.F. Wu, Y.L. Li, Effects of dual-frequency ultrasound with different energy irradiation modes on the structural and emulsifying properties of soy protein isolate, Food Bioprod. Process. 123 (2020) 419–426, https://doi.org/10.1016/j.fbp.2020.07.021.

[47] X.B. Ma, W.J. Wang, M.M. Zou, T. Ding, X.Q. Ye, D.H. Liu, Properties and structures of commercial polygalacturonase with ultrasound treatment: role of ultrasound in enzyme activation, RSC Adv. 5 (2015) 107591–107600, https://doi.org/10.1039/C5RA19425C.

[48] B. Wang, T.T. Meng, H.L. Ma, Y.Y. Zhang, Y.L. Li, J. Jin, et al., Mechanism study of dual-frequency ultrasound assisted enzymolysis on rapeseed protein by immobilized Alcalase, Ultrason. Sonochem. 32 (2016) 307–313, https://doi.org/10.1016/j.ultsonch.2016.03.023.